Sensors and Materials, Vol. 35, No. 1 (2023) 103–120
MYU Tokyo

S & M 3157

Method of Extracting Respiration Rate and Heartrate by Ultra-wideband Radar for Human Monitoring

Xu Jingbo,[1*] Xu Xiaohong,[2] Li Qiaowei,[1] Ma Wenbo,[1] and Zhang Fujun[1]

[1]School of Measurement–Control Technology and Communication Engineering, Harbin University of Science and Technology, 52, Xuefu Road, Harbin 150080, China
[2]Department of Textile Engineering, Shazhou Professional Institute of Technology, 1, Fuxin Road, Zhangjiagang 215627, China

(Received August 29, 2022; accepted January 6, 2023)

Keywords: UWB radar, respiration rate, heartrate, wavelet, FFT

Because of the noteworthy characteristics of ultra-wideband (UWB) radar, it has been applied in the noncontact measurement of vital signs. The fluctuating movement of the chest caused by respiration and heartbeat of the human body is comprehensively reflected in the radar echo. A key problem is how to separate respiration and heartrate signals in the echo then evaluate the vital sign parameters. In this study, the position of a monitored object is judged from the output data frame of the radar, then the data sequence of chest movement in the time domain is extracted. The signal is filtered by the wavelet threshold method using the sym6 wavelet basis function, then the spectrum of the denoised signal is analyzed. This method can effectively extract the respiration rate and heartrate and achieve real-time monitoring. Its feasibility and effectiveness were verified by several sets of experiments, which indicate that the method can be applied in practice. This method is expected to help popularize the use of UWB radar in medical monitoring.

1. Introduction

In the monitoring of human vital signs, respiration rate and heartrate are two important indicators. Through the monitoring of these two parameters, changes in vital signs can be rapidly detected, saving time and lives. In addition, in rescue work after major accidents, the respiration rate and heartrate can also help indicate the existence of survivors, providing a powerful way of detecting bodies. The traditional measurement of human respiration rate and heartrate generally relies on a contact detection method, and the adopted instruments and equipment include sphygmomanometers, electrocardiogram (ECG) recorders, smart wristbands, and breathing bandages. Such equipment is not suitable for some special groups, such as elderly people, infants, and severely burned patients. Because of the decreased weight of elderly people, the installation and use of contact equipment become difficult, for example, the equipment may easily become detached, which is detrimental to the monitoring of vital signs and results in a poor experience for the tested person. For infants and patients with severe burns, instruments in

*Corresponding author: e-mail: hitxjb@126.com
https://doi.org/10.18494/SAM4066

ISSN 0914-4935

direct contact with their bodies not only restricts their body activities but also causes secondary injuries. Thus, noncontact measurement is very important for such groups.

For the noncontact checking of vital signs, IR rays, ultrasonic waves, biological radar, and other methods are usually adopted. Because biological radar, especially ultra-wideband (UWB) radar, emits electromagnetic waves, its penetration ability is very strong; weather, temperature, humidity, dress material, and other external factors have little influence on this method, making it ideal for checking vital signs. In bio-radar, separating the respiration rate and heartrate components from the radar echo signal and extracting the corresponding parameters are key technologies. Traditional methods include bandpass filtering, the short-time Fourier transform (STFT), the power spectrum method, and adaptive filtering.[1–3] Because the frequency bands of respiration and heartbeat are relatively close, and the filter in the frequency domain has a narrow transition band and a passband ripple, such a filter cannot effectively separate the signals. The STFT transforms the signal by moving a window function along the time axis. The shorter the time window, the better the time resolution will be. However, a shorter time window leads to poor frequency resolution and even failure to obtain the signal frequency. The STFT cannot change the window adaptively, which limits its application in the time-frequency analysis of radar signal processing or monitoring different targets. The power spectrum of the signal is actually the Fourier transform of the signal autocorrelation function. The autocorrelation operation can effectively retain the periodic signals and suppress noise interference; thus, the periodic signals of respiration and heartbeat in radar echo will be retained and their periods will remain unchanged. However, the power spectrum algorithm introduces some error into the obtained signal frequency. For the adaptive filtering method, the input signals of the system model are the body motion signal (mainly composed of respiration and heartbeat signals) detected by biological radar and the respiration signal. The respiration signal is input to the adaptive filter as a reference signal. The recursive least squares algorithm (RLS) automatically adjusts the weight coefficients of the filter according to the error between the output of the adaptive filter and the body motion signal. When the error is minimized, the algorithm stops. At this time, the output of the model is just the heartbeat signal. In this approach, the reference respiration signal is obtained using a low-pass filter, and it cannot accurately reflect the movements of the chest caused by breathing.

Focusing on the characteristics of UWB radar echo of a large background noise and a heartbeat signal that is weak and difficult to extract, in this paper, we propose a processing method combining adaptive wavelet filtering and the fast Fourier transform (FFT). The adaptive threshold denoising strategy effectively removes the interference noise based on an unbiased risk estimate, making the subsequent heartrate extraction and calculation more robust and accurate. The amplitude of the signal in the frequency domain is obtained through the FFT, and then the respiration rate and heartrate are extracted.

2. Principle of UWB Radar

Compared with continuous-wave radar, UWB pulse radar has a higher positioning accuracy and can detect vital signs such as heartbeat and respiration rate more accurately, and the echo

signal of UWB radar can carry more information on vital signs, making it more suitable for the medical field.[4–7]

As illustrated in Fig. 1, the basic principle of UWB radar is that it generates continuously pulsed electromagnetic waves, which are amplified by a power amplifier and transmitted through a transmission antenna. The electromagnetic waves are reflected when they meet the monitored human body, in which the original signal is modulated by the breathing-induced movement of the chest, inducing the Doppler effect and producing an echo signal. After the echo signal is picked up by a receiving antenna and preprocessed by a low-noise amplifier, an analog-to-digital converter, and a control unit, the distance from the radar to the monitored human and the information on the chest displacement can be obtained. The acquired original data are transmitted to the main computer for processing by separation and extraction algorithms, so as to obtain the information on vital signs contained in the echo signal.[8,9]

An electromagnetic wave travels through air at a speed close to the speed of light, and the detection range can be determined from the time difference between its emission and reflection using the following equation.

$$s_0 = \frac{1}{2} c t_d \tag{1}$$

Here, s_0 denotes the distance to the measured object, c denotes the propagation velocity of the electromagnetic wave, and t_d denotes the time difference between the emission and reflection of the electromagnetic wave.

The fluctuating movement of the human chest is related to respiration and heartbeat, among which respiration plays the major role. The fluctuation range of the chest is 0 to 3 cm during respiration. The heartbeat can also cause slight fluctuation of the chest with an amplitude range of 1.5 to 3.5 mm.[9,10] Both signals are periodic and are superimposed. Thus, the distance detected by the radar targeted at the object is changing continuously under the influence of chest movement, which is modeled by the following equation.

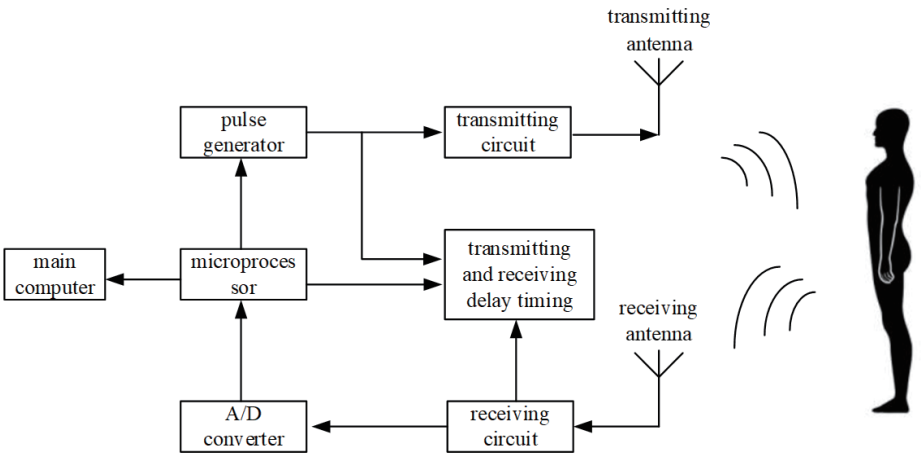

Fig. 1. Principle of UWB radar.

$$s(t) = s_0 - ud_1(T_1) - vd_2(T_2) \tag{2}$$

Here, u denotes the amplitude of chest fluctuation caused by respiration, T_1 denotes the respiration period, v denotes the amplitude of chest fluctuation caused by the heartbeat, and T_2 denotes the heartbeat period. u and v are the amplitude of chest rise and fall caused by the breathing and heartbeat. The chest moves constantly and its displacement can be detected by radar. The respiration and heartrate information contained in the displacement can be separated and extracted by the method proposed in the following section.

3. Data Acquisition from Radar Echo Signal

3.1 Acquisition of human body motion data

In this study, an X4M02 UWB biological radar module produced by XETHRU is used to collect the signals of human respiration and heartbeat. The sampling rate of the X4M02 module is 23.328 GS/s, and a single acquisition contains 1536 data points. Because an electromagnetic wave travels at the speed of light, which is 300000 km/s, a distance of about 9.9 m can be detected during a single sampling time. The acquisition experiment performed in this study is shown in Fig. 2. The module is mounted on a support and connected with a computer through a USB data cable. The height of the support is adjusted according to the monitored object. After the computer enables the module to collect signals, the module transmits the pulse signal continuously. After the pulse signal meets the measured human body, it is reflected and generates an echo signal. The module collects the echo signal at this time and saves the data in the computer. Finally, a MATLAB program in the computer is used to play back the echo signal, process the data, and extract the information on vital signs.

In the data acquisition experiment, the X4M02 module reduces the intensity of the echo signal by a factor of eight and outputs data in the form of a data frame with a frequency of 20 Hz. The amplitude of the echo signal in a single frame is shown in Fig. 3. The horizontal axis represents 192 sampling points, corresponding to a distance of 9.9 m, and the horizontal resolution is 5.2 cm/point. For example, the 35th point corresponds to 2 m. The vertical axis represents the amplitude of each position in the echo signal in the normalized form, where the stronger the reflected signal, the higher the amplitude.

Fig. 2. Data acquisition experiment.

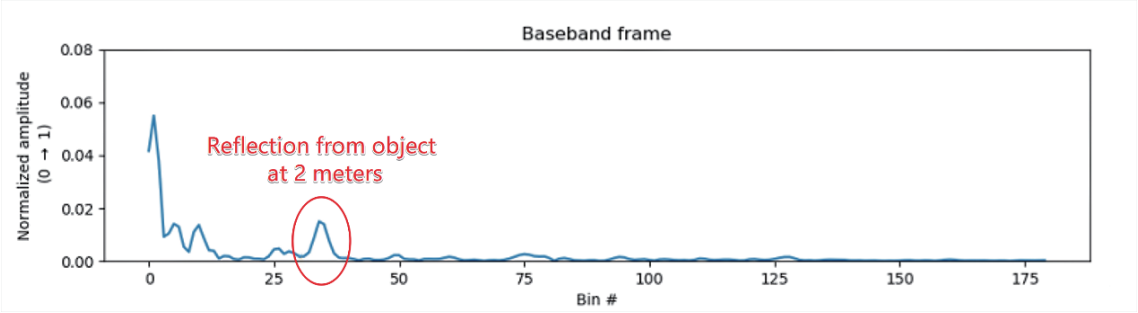

Fig. 3. (Color online) One frame of radar echo data.

3.2 Data frame extraction and reconstruction

To effectively analyze the echo signal of the monitored person, it is necessary to extract it at the sampling interval to obtain time series data of the target point. In other words, each output frame of radar is extracted according to the position index of the target point in the frame to form a new time-domain data series for signal analysis of the monitored person.

From the above analysis, it can be seen that the location of the target point is critical and directly affects the extraction of data. Because of the influence of the chest fluctuation, the echo signal of the target point shows periodic fluctuation among different frame sequences, as shown in Fig. 4. On the basis of this characteristic, the position of the monitored target can be determined. Therefore, by calculating the range of the amplitude of each sampling point, that is, the difference between the maximum and minimum values, and judging its periodicity, the distance and position of the monitored person relative to the radar can be determined.

After each data frame is extracted, the extraction points of different frames are reconstructed in chronological order to form a new time-domain sequence, which represents the change in human chest displacement with time. The sampling frequency of this new data sequence is the frame frequency of UWB radar, which contains displacement information such as human respiration and heartbeat. The whole process is shown in Fig. 5.

4. Wavelet Denoising for Radar Echo Signal

The processing of time-domain series data for a radar echo signal mainly includes signal denoising, spectrum analysis, and frequency extraction of the respiration rate and heartrate. Because the frequency bands of the respiration rate and heartrate are adjacent and contain noise, it is difficult to separate them by frequency domain filtering. In this study, a wavelet filtering method is adopted, which can effectively retain the spikes and singularities of a valid signal. Then, the denoised time-domain series data are transformed to the frequency domain to extract the feature points of the spectrum and calculate the respiration rate and heartrate. A flow chart of the algorithm is shown in Fig. 6.

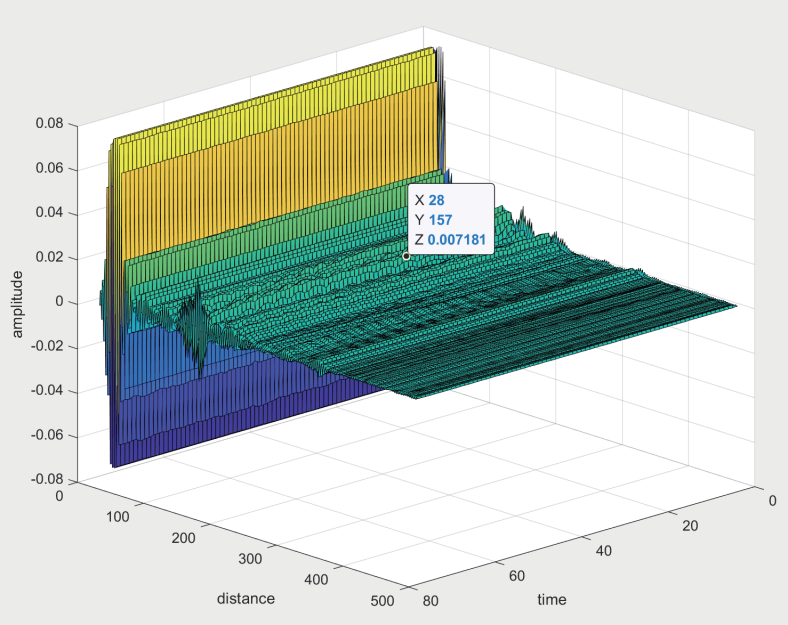

Fig. 4. (Color online) Data frame in time and space.

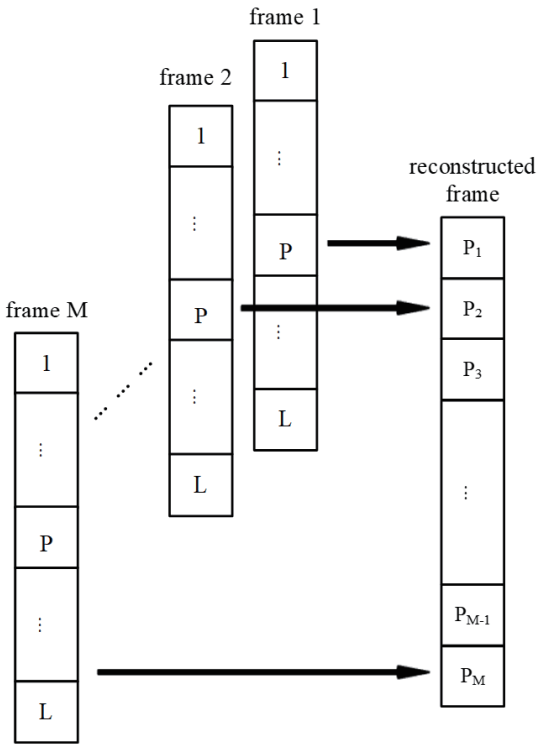

Fig. 5. Data extraction and reconstruction in frames.

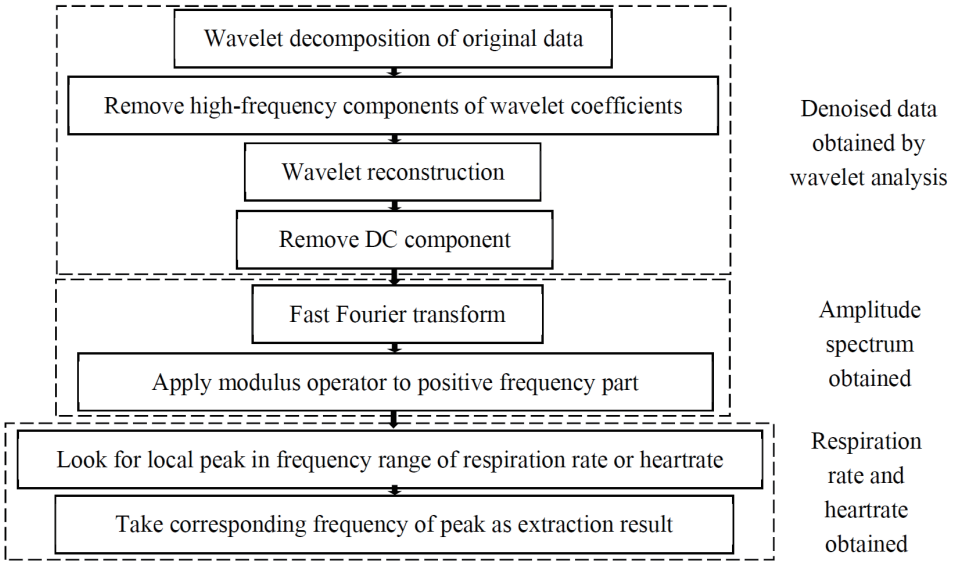

Fig. 6. Flow chart of the algorithm for respiration rate and heartrate extraction.

In this study, the wavelet threshold denoising method is adopted. Because the amplitude of the wavelet coefficients of useful signals is significantly larger than that of the noise after wavelet decomposition, the noise contained in the signal can be suppressed effectively. The specific data processing is as follows. Firstly, the noisy signal is decomposed by an orthogonal wavelet at each scale, and the large-scale (low-resolution) decomposition coefficients are retained. Secondly, a threshold is set for other decomposition coefficients with a small scale (high resolution). The coefficients below this threshold are set to zero, and those higher than this threshold are either left intact or processed as "shrinkage". Finally, the signal is reconstructed on the basis of these processed wavelet coefficients by using the inverse wavelet transform. This transform removes high-frequency components in the signal and retains the information included in the low-frequency band containing the respiration rate and heart rate, so as to restore the effective signal.

4.1 Wavelet decomposition and reconstruction of signal

According to wavelet analysis theory, a signal can be decomposed and reconstructed in a series of scale spaces V_j and detail spaces W_j. When $f_j \in V_j$, it can be decomposed into

$$f_j = f_{j+1} + w_{j+1}, f_{j+1} \in V_{j+1}, w_{j+1} \in W_{j+1}, \tag{3}$$

where

$$f_{j+1} = \sum_{n \in Z} A_{j+1}(n)\varphi_{j+1}(n), w_{j+1} = \sum_{n \in Z} D_{j+1}(n)\psi_{j+1}(n).$$

Here, A denotes the smoothing coefficients, D denotes the detail coefficients, φ denotes scaling functions, and ψ denotes wavelet functions.

Furthermore, through the fast multiresolution extraction of a signal, signals in different frequency ranges can be obtained, which are subjected to multiscale analysis.[11,12] In the frequency domain analysis, the wavelet function can be considered as a bandpass filter, which is equivalent to a high-pass filter h and a low-pass filter g in series. For cascaded filters of different passbands, the Mallat algorithm can be used to decompose and reconstruct the signal at different scales, and the decomposition process is shown in Fig. 7.

The discrete wavelet decomposition process can be described as

$$A_{j+1}(n) = \sum_{m=-\infty}^{\infty} A_j(m)\bar{h}(m-2n), \tag{4}$$

$$D_{j+1}(n) = \sum_{m=-\infty}^{\infty} A_j(m)\bar{g}(m-2n), \tag{5}$$

where h denotes the low-pass filter, g denotes the high-pass filter, and A_0 denotes the original signal. These equations describe the relationship between the smoothing coefficients and detail coefficients at different scales.

Its inverse transformation process, namely, the wavelet reconstruction process, is shown in Fig. 8. The discrete wavelet reconstruction process can be described as

$$A_j(n) = \sum_{m=-\infty}^{\infty} A_{j+1}(m)h(n-2m) + D_{j+1}(m)g(n-2m). \tag{6}$$

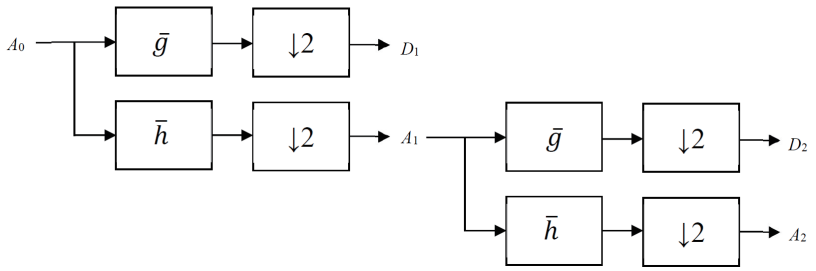

Fig. 7. Mallat pyramidal algorithm for signal decomposition.

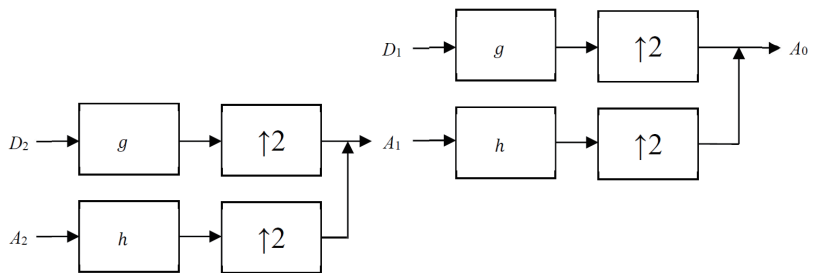

Fig. 8. Mallat pyramidal algorithm for signal reconstruction.

In the same way, the signal can be reconstructed using Eq. (3). For the filtering application, the detail coefficients corresponding to the removed components should to be set to 0.

The sym6 wavelet base function is adopted in this study. The coefficients of the low-pass and high-pass filters used for decomposition and reconstruction are shown in Table 1. The optimal number of wavelet decomposition layers is determined to be four, then the noisy signal is processed at each scale. The sym6 wavelet is orthogonal with quasi-symmetry, making it an improvement of the Daubechies wavelet, and it also has minimal phase distortion and very good symmetry. The wavelet decomposition processing of the simulated signal is shown in Fig. 9.

Table 1
Coefficients of low-pass and high-pass filters used for decomposition and reconstruction.

Items	*k*											
	1	2	3	4	5	6	7	8	9	10	11	12
Low-pass filter for decomposition	0.0154	0.0035	0.1180	−0.0483	0.4911	0.7876	0.3379	−0.0726	−0.0211	0.0447	0.0018	−0.0078
High-pass filter for decomposition	0.0078	0.0018	−0.0447	−0.0211	0.0726	0.3379	−0.7876	0.4911	0.0483	−0.1180	−0.0035	0.0154
Low-pass filter for reconstruction	−0.0078	0.0018	0.0447	−0.0211	−0.0726	0.3379	0.7876	0.4911	−0.0483	−0.1180	0.0035	0.0154
High-pass filter for reconstruction	0.0154	−0.0035	−0.1180	0.0483	0.4911	−0.7876	0.3379	0.0726	−0.0211	−0.0447	0.0018	0.0078

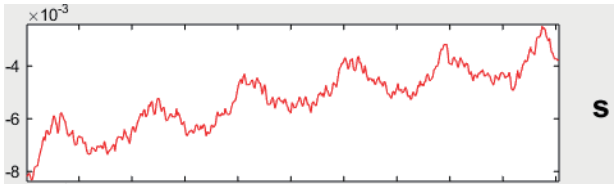

(a)

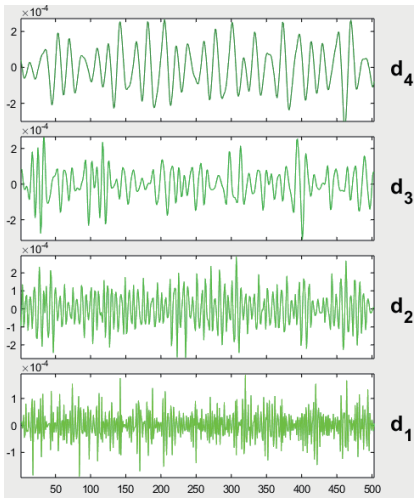

(b)

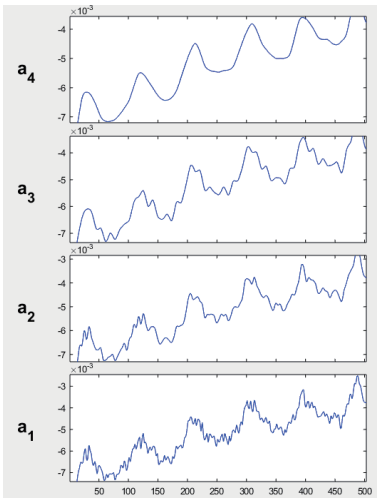

(c)

Fig. 9. (Color online) Wavelet decomposition process. (a) Original signal s, (b) detailed coefficients of wavelet decomposition d_1–d_4, and (c) approximation coefficients of wavelet decomposition a_1–a_4.

4.2 Wavelet threshold denoising

A soft threshold method is used to process the decomposed wavelet coefficients of each layer, that is, coefficients greater than the threshold are retained by subtracting them from the threshold, whereas coefficients less than the threshold are set to zero.[13,14]

Unbiased risk estimation is used to determine the threshold, that is, each element of the wavelet decomposition coefficient $d(n)$ is changed to an absolute value, then these absolute values are sorted from small to large. Finally, these absolute values are squared to obtain a new signal sequence $f(k)=\left(sort\left(|d|\right)\right)^2$. If the square root of the kth element is taken as the threshold, the threshold should be $\lambda_k=\sqrt{f(k)}$, where $k = 0, 1, 2, ..., n - 1$.

Accordingly, the risk generated by this threshold is

$$Risk(k)=\frac{\left[n-2k+\sum_{j=1}^{k}f(j)+(n-k)f(k)\right]}{n}. \tag{7}$$

A risk curve for $Risk(k)$ can be formed using Eq. (7), the minimum value index of which is taken as k_{min}, and the unbiased risk estimation threshold is exactly $\lambda=\sqrt{f\left(k_{min}\right)}$.

In this way, soft threshold processing can be performed. The relationship between the absolute value of the wavelet coefficient $|d|$ and the threshold λ is

$$d_\lambda=\begin{cases}\left[\mathrm{sgn}(d)\right]\left(|d|-\lambda\right), & |d|\geq\lambda\\ 0, & |d|<\lambda\end{cases} \tag{8}$$

where $\mathrm{sgn}(d)$ is the sign function, that is, $\mathrm{sgn}(d)$ is 1 when d is positive, −1 when d is negative, and 0 when d is 0. For example, for a certain frame data, the decomposition thresholds of the first and second layers, $d_{1\lambda}$ and $d_{2\lambda}$, are calculated to be 1.4959×10^{-4} and 5.1463×10^{-4}, respectively.

Finally, the inverse wavelet transform is used to reconstruct the signal from the retained coefficients to obtain the denoised signal. The denoising effect is shown in Fig. 10. It can be seen that the high-frequency noise in the original signal is effectively eliminated.

5. Amplitude Spectrum Analysis

The denoised signal is converted to the frequency domain for amplitude frequency analysis through the discrete Fourier transform (DFT):

$$F(\omega)=\sum_{n=0}^{N-1}f(n)e^{-j\omega n}, \tag{9}$$

where $f(n)$ is the denoised signal, $F(\omega)$ is its DFT, and the amplitude frequency characteristic of $F(\omega)$ is obtained by taking its modulus. To improve the computing efficiency, the FFT is adopted.

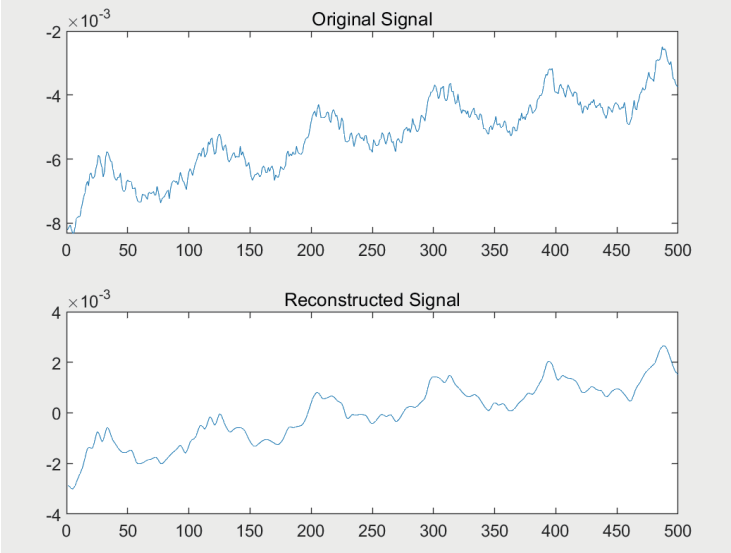

Fig. 10. (Color online) Comparison of original and reconstructed signals.

Firstly, the FFT is performed on the reconstructed signal, and the modulus of the signal is taken in the frequency domain to obtain the amplitude frequency characteristics.[15,16] The obtained amplitude spectrum curve is shown in Fig. 11. There is a clear local peak at 0.24 Hz, and the signal amplitude at this point is relatively strong, clearly indicating that the reconstructed signal contains this frequency component. By comparison with the range of the human respiration rate, it can be judged that the frequency at this point represents the respiration frequency of the monitored person. In addition, there is another local peak at a frequency of 1.04 Hz, which can be judged to be the heartbeat frequency.

Therefore, local maximum peaks of the respiration rate and heartrate signals are found within their respective frequency ranges in the amplitude spectrum, namely, the respiration rate and heartrate signals. Since the horizontal coordinate of the amplitude spectrum represents the frequency, the two signals should be converted into beats per minute (BPM), and the following final results are obtained.

$$\text{Respiration rate: } 0.24 \times 60 = 14.4 \text{ RPM}$$
$$\text{Heartrate: } 1.04 \times 60 = 62.4 \text{ BPM}$$

This method is compared with the traditional bandpass filter and STFT methods for different test objects, as shown in Fig. 12. In some cases, the extraction of the respiratory rate and heart rate by the bandpass filter is insufficiently accurate. The STFT has poor heartrate extraction performance, whereas the proposed method has high robustness. It also performs well when the subject is talking.

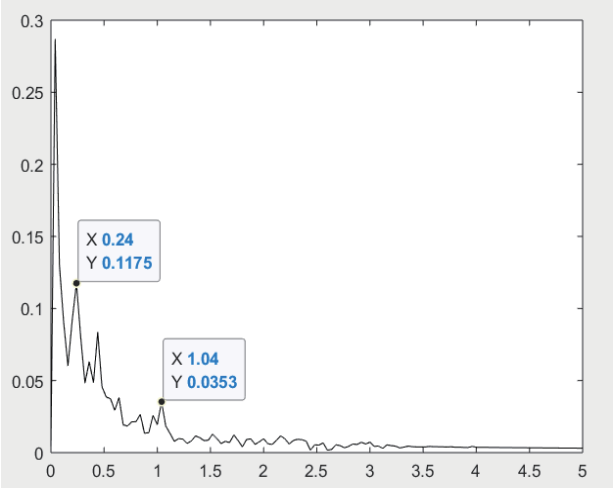

Fig. 11. (Color online) Amplitude spectrum of the reconstructed signal.

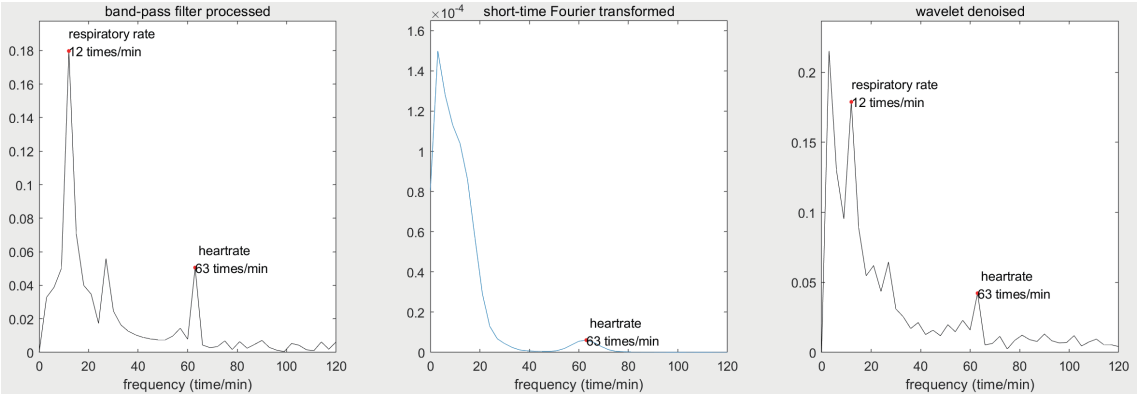

(a)

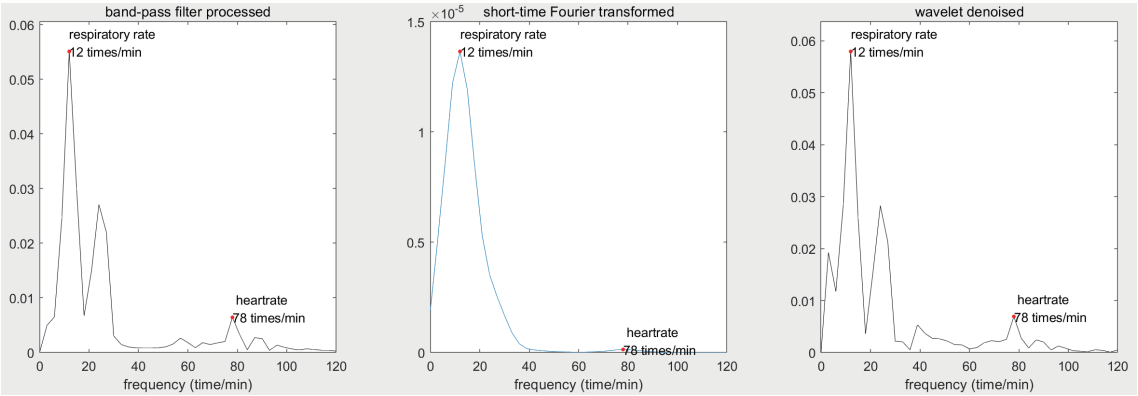

(b)

Fig. 12. (Color online) Comparison of different methods. (a) The actual respiratory rate of the subject is 12 times per minute and the heartrate is 63 times per minute. (b) The actual respiratory rate of the subject is 12 times per minute and the heartrate is 78 times per minute. (c) The actual respiratory rate of the subject is 18 times per minute and the heartrate is 72 times per minute. (d) The actual respiratory rate of the subject while talking is 24 times per minute and the heartrate is 80 times per minute.

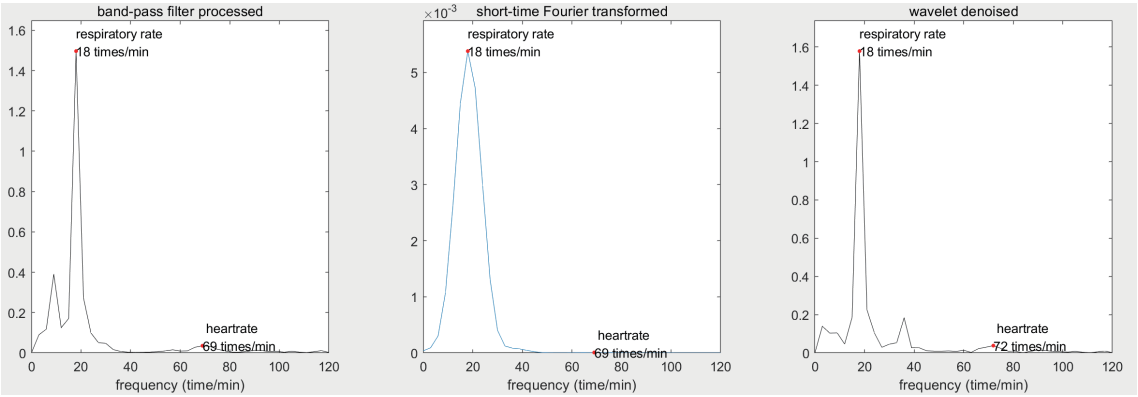

(c)

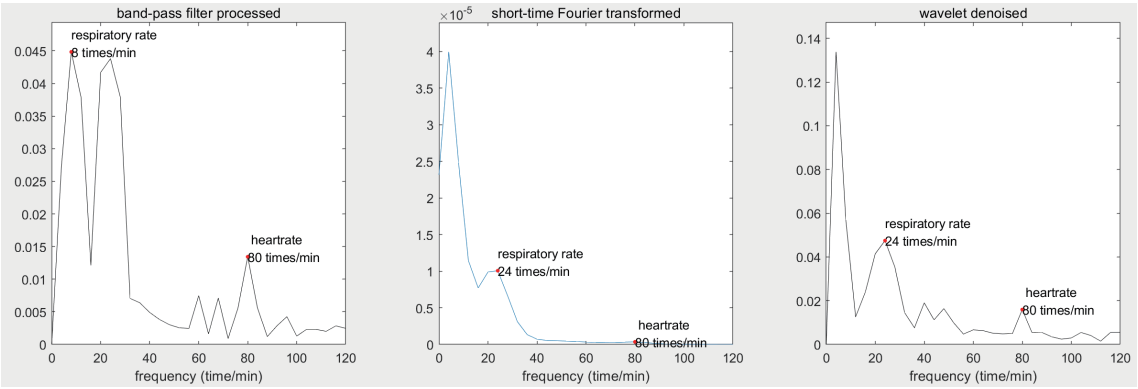

(d)

Fig. 12. (Color online) (Continued) Comparison of different methods. (a) The actual respiratory rate of the subject is 12 times per minute and the heartrate is 63 times per minute. (b) The actual respiratory rate of the subject is 12 times per minute and the heartrate is 78 times per minute. (c) The actual respiratory rate of the subject is 18 times per minute and the heartrate is 72 times per minute. (d) The actual respiratory rate of the subject while talking is 24 times per minute and the heartrate is 80 times per minute.

6. Experiment

6.1 Experimental procedure

To evaluate the reliability and consistency of the algorithm, a controlled variable approach was applied in the experiment. Data were collected from multiple subjects under different conditions, such as in the sitting and quietly lying states after exercise. The sampling frequency per frame of radar was 20 Hz.

The algorithm programmed by MATLAB script was used to extract the respiration rate and heartrate from the original data. The interface and functions of the software are shown in Fig. 13, which includes three subplots of the curve. The subplot at the top shows the original

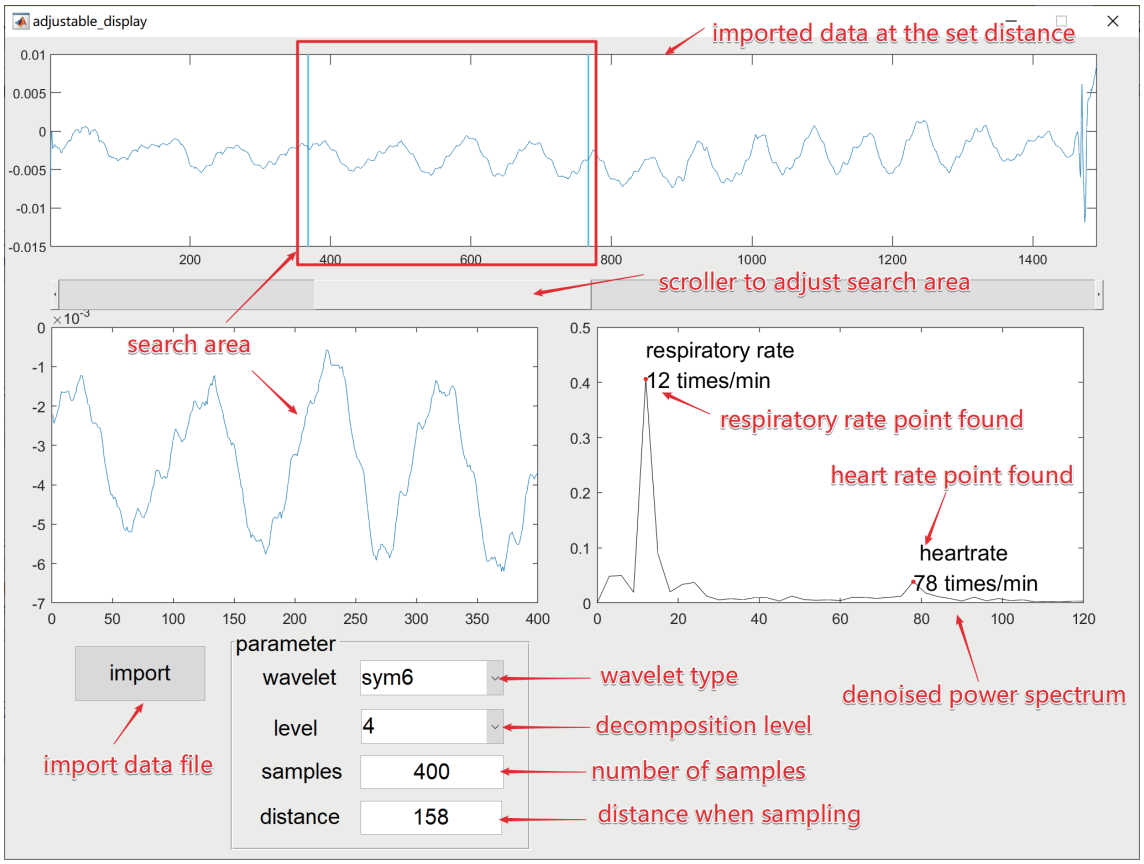

Fig. 13. (Color online) Software interface used for radar signal processing and information extraction.

data, the subplot on the middle left shows the sampled original data to be processed, and the subplot on the middle right shows the extraction results of the respiration rate and heartrate. As shown at the bottom of Fig. 13, there are buttons for importing the data and for parameter setting, including the selection of the wavelet function and the wavelet decomposition layers and the selection of the sampling points. After the original data are imported and the parameters are set, the sampling range of the data is selected by dragging the scroll bar below the original data subplot. Two vertical line marks above the scroll bar correspond to the selected range. The size of the scroll bar automatically scales with the number of sampling points, and the sampling data subplot and the extraction result subplot change with the parameters and the scroll bar in real time.

During the measurement, a wrist blood pressure and pulse meter was used to measure the heartrate of the monitored person, which was used as the reference value of the heartrate. The participant counted his breaths in one minute by himself to obtain the reference value of the respiration rate. The measurement results obtained by the proposed method were compared with the reference values to verify the accuracy of the algorithm.

In the experiment, the measurement results of the same object in different periods and different sampling points were compared to evaluate the consistency of the algorithm, and the

influence of different sampling points on the measurement results was also analyzed. The effectiveness and universality of the algorithm were evaluated by comparing the measurement results of different participants.

6.2 Analysis of experimental results

A total of nine groups of data were collected from three people in the sitting and lying states. Table 2 shows the measurement results of person A in the sitting state after exercise obtained using different sampling points. The reference heartrate was 75 times/min and the reference respiration rate was 14 times/min. Table 3 shows the measurement results of person A in the quietly lying state after exercise using different sampling points. The reference heartrate was 63 times/min and the reference respiration rate was 12 times/min.

The accuracy was used to evaluate the consistency between the measurement results and the reference values, and the root mean square error (RMSE) was used to evaluate the stability of the measurement results for different sampling points. The formulas for the accuracy and RMSE are

$$accuracy = 1 - \frac{1}{n}\frac{\sum \mathrm{abs}(Est - Ref)}{Ref}, \tag{10}$$

$$RMSE = \sqrt{\frac{\sum (Est - Ref)^2}{n}}, \tag{11}$$

Table 2
Sampling points and measurement results for person A in sitting state.

Items	Testing results				
	200 sampling points	250 sampling points	300 sampling points	350 sampling points	400 sampling points
Heartrate (Times/min)	72	77	76	75	75
	72	77	76	75	75
	72	72	72	75	75
	78	72	76	75	75
	72	77	76	75	75
	78	77	76	75	75
	72	77	76	75	75
	78	77	76	75	75
Respiration rate (Times/min)	12	14	12	14	12
	12	14	12	14	15
	12	14	16	14	15
	12	14	16	14	15
	12	14	16	14	15
	12	14	16	14	15
	12	14	16	14	15
	12	14	16	14	15

Table 3
Sampling points and measurement results for person A in lying state.

Items	Testing results				
	200 sampling points	250 sampling points	300 sampling points	350 sampling points	400 sampling points
Heartrate (Times/min)	60	62	64	62	63
	66	62	64	62	63
	60	62	64	62	63
	60	58	64	62	63
	60	62	64	62	63
	66	62	64	62	63
	60	62	64	65	63
	60	62	64	62	63
Respiration rate (Times/min)	12	14	12	14	12
	12	14	12	14	12
	18	14	12	14	12
	12	14	12	14	12
	12	14	12	14	12
	12	14	16	14	12
	12	14	12	14	12
	12	14	12	14	12

Table 4
Measurement results for person A in sitting state for different numbers of sampling points.

Items	Testing results				
	200 sampling points	250 sampling points	300 sampling points	350 sampling points	400 sampling points
Heartrate accuracy (%)	96.3	96.3	97.3	98.6	98.6
Respiration rate accuracy (%)	85.7	100.0	85.7	100.0	92.0
Heartrate RMSE (BPM)	2.92	2.78	2.00	1.00	1.00
Respiration rate RMSE (RPM)	2.00	0.00	2.00	0.00	1.17

Table 5
Measurement results for person A in lying state for different numbers of sampling points.

Items	Testing results				
	200 sampling points	250 sampling points	300 sampling points	350 sampling points	400 sampling points
Heartrate accuracy (%)	95.2	97.6	98.4	98.2	100.0
Respiration rate accuracy (%)	93.8	83.3	95.8	83.3	100.0
Heartrate RMSE (BPM)	3.00	2.00	1.00	1.17	0.00
Respiration rate RMSE (RPM)	2.12	2.00	1.41	2.00	0.00

Table 6
Relationship between the mean value of measurement results and sampling points.

Items	Testing results				
	200 sampling points	250 sampling points	300 sampling points	350 sampling points	400 sampling points
Average heartrate accuracy of multiple groups (%)	95.2	97.1	97.7	97.7	98.9
Average respiration rate accuracy of multiple groups (%)	90.5	90.1	92.8	90.5	94.2
Average heartrate RMSE of multiple groups (BPM)	4.89	2.93	2.61	2.14	1.13
Average respiration rate RMSE of multiple groups (RPM)	1.87	1.37	1.28	1.35	0.97

where n is the number of measurements, *Est* denotes the measurement result, and *Ref* denotes the reference value.

Tables 4 and 5 show the accuracy and RMSE of the measurement results in Tables 2 and 3, respectively. It can clearly be seen that the measurement results of heartrate and respiration rate are affected by the number of sampling points, and the more sampling points, the greater the stability. The accuracy of the heartrate showed a slightly positive correlation with the number of sampling points, whereas the accuracy of the respiration rate was not significantly affected by the number of sampling points.

The remaining seven groups of data were processed by the above method, and the heartrate accuracy, respiration rate accuracy, average heartrate RMSE, and average respiration rate RMSE for the nine sets of data were calculated, as shown in Table 6. It can be seen that the accuracy of both the heartrate and respiration rate generally increases whereas the RMSE decreases with increasing number of sampling points. This indicates that the greater the number of sampling points, the more stable the measurement results tend to be, but the real-time performance of data processing decreases. We found that 400 sampling points is an appropriate number of sampling points for which good measurement results can be obtained by collecting valid data for about 20 s with 20 Hz frame frequency.

7. Conclusions

We studied an algorithm for extracting the respiration rate and heartrate from a UWB radar echo signal. Using wavelet denoising and the FFT method, we effectively obtained the vital sign parameters of the respiration rate and heartrate of the monitored person. In the algorithm, the sym6 wavelet function, four decomposition layers, four reconstruction layers, and 400 sampling

points were selected. The accuracy, consistency, and effectiveness of the algorithm were verified by performing multiple groups of experiments with different monitored people.

Using UWB radar to obtain the information of human vital signs has the advantage of non-contact measurement. We have provided a practical signal extraction algorithm that effectively solves the problem of separating and extracting the respiration rate and heartrate in a radar echo signal. This algorithm can be extended to the application of UWB radar in medical treatment and daily monitoring, giving it broad application prospects.

Acknowledgments

The theoretical analysis, data acquisition, programming, and experiment in this work were supported by all members of the research group. The paper was supported by Harbin Science and Technology Plan self-funded project (2022ZCZJCG004).

References

1 T. Q. Chen, Y. Q. Zhang, B. C. Zong, and Z. Q Tian: Chin. J. Med. Instrum. **45** (2021) 188. https://doi.org/10.3969/j.issn.1671-7104.2021.02.014
2 L. Y. Ren, Y. S. Koo, H. F. Wang, Y. Z. Wang, Q. H. Liu, and A. E. Fathy: IEEE Microwave Wireless Compon. Lett. **25 (**2016) 690. https://doi.org/10.1109/LMWC.2015.2463214
3 X. C. Dang, J. L. Zhang, Z. J. Hao, and Y. An: Comput. Eng. **47** (2021) 175. https://doi.org/10.19678/j.issn.1000-3428.0060078
4 F. Soldovieri, I. Catapano, L. Crocco, L. N. Anishchenko, and S. I. Ivashov: Int. J. Antennas Propag. **12** (2014) 1072. https://doi.org/10.1155/2012/420178
5 L. Y. Ren, H. F. Wang, K. Naishadham, O. Kilic, and A. E. Fathy: IEEE Trans. Microwave Theory Tech. **64** (2016) 1. https://doi.org/10.1109/TMTT.2016.2597824
6 N. Andersen, K. Granhaug, J. A. Michaelsen, S. Bagga, H. A. Hjortland, M. R. Knutsen, T. S. Lande, and D. T. Wisland: IEEE J. Solid-State Circuits **52** (2017) 3421. https://doi.org/10.1109/JSSC.2017.2764051
7 X. K. Hu and T. Jin: J. Radars. **5** (2016) 462. https://doi.org/10.12000/JR16103
8 J. Bai, D. S. Huang, X. Zhang, and P. F. Zhang: Chin. Med. Equip. J. **35** (2014) 10. https://doi.org/10.7687/J.ISSN.1003-8868.2014.03.010
9 F. Yang, H. Zhang, S. Li, H. J. Xue, and G. H. Lu: Chin. Med. Equip. J. **35** (2014) 28. https://doi.org/10.7687/J.ISSN.1003-8868.2014.07.028
10 C. Z. Gu and C. Z. Li: Sensors **15** (2015) 6383. https://doi.org/10.3390/S150306383
11 L. Yi, Y. G. He, G. F. Fang, and X. T. Fan: Appli. Res. Comput. **30** (2013) 172. https://doi.org/10.3969/j.issn.1001-3695.2013.01.044
12 H. H. Maria, A. M. Jossy, G. Malarvizhi, and A. Jenitta: Optik **241** (2021) 1. https://doi.org/10.1016/j.ijleo.2021.166883
13 Z. K. Xu, Z. Y. Wang, S. Y. Bai, Y. Zhang, and H. J. Xue: Chin. Med. Equip. J. **42** (2021) 1. https://doi.org/10.19745/j.1003-8868.2021201
14 B. Fang, J. Y. Chen, and Y. Shi: Opt. Tech. **47** (2021) 359. https://doi.org/10.13741/j.cnki.11-1879/o4.2021.03.018
15 X. M. Li, X. P. Wang, R. G. Qi, and G. A. Bi: Digital Signal Process. **117** (2021) 1. https://doi.org/10.1016/j.dsp.2021.103136
16 J. C. Yang and L. A. Liu: Electron. Lett. **54** (2018) 901. https://doi.org/10.1049/el.2018.0739